Applied Catalysis B: Environmental 226 (2018) 534–543

Contents lists available at ScienceDirect

Applied Catalysis B: Environmental

journal homepage: www.elsevier.com/locate/apcatb

NiCu single atom alloys catalyze the C—H bond activation in the selective non- oxidative ethanol dehydrogenation reaction

Junjun Shan[a,b], Jilei Liu[a], Mengwei Li[a], Sylvia Lustig[a], Sungsik Lee[c], Maria Flytzani-Stephanopoulos[a,*]

[a] Department of Chemical and Biological Engineering, Tufts University, Medford, MA, 02155, USA
[b] Present address: NICE America Research, Inc, Mountain View, CA, 94043, USA
[c] X-ray Science Division, Argonne National Laboratory, 9700 South Cass Avenue, Argonne, IL, 60439, USA

ARTICLE INFO

Keywords:
Single atom alloys
Copper
C-H bond activation
Nickel
Ethanol dehydrogenation

ABSTRACT

NiCu single atom alloy (SAA) nanoparticles supported on silica are reported to catalyze the non-oxidative dehydrogenation of ethanol, selectively to acetaldehyde and hydrogen products by facilitating the C—H bond cleavage. The activity and selectivity of the NiCu SAA catalysts were compared to monometallic copper and to PtCu and PdCu single atom alloys, in a flow reactor at moderate temperatures. *In-situ* DRIFTS showed that the silica support facilitates the O—H bond cleavage of ethanol to form ethoxy intermediates over all the supported alloy catalysts. However, these remain unreactive up to 250 °C for the Cu/SiO_2 monometallic nanoparticles, while in the NiCu SAA, acetaldehyde is formed at much lower temperatures, below 150 °C. *In situ* DRIFTS was also used to identify the C—H activation step as the rate determining step of this reaction on all the copper catalysts we examined. The presence of atomically dispersed Ni in Cu significantly lowers the C—H bond activation barrier, whereas Pt and Pd atoms were found less effective. This work provides direct evidence that the C—H bond cleavage is the rate determining step in ethanol dehydrogenation over this type catalyst.

1. Introduction

Acetaldehyde is an important chemical intermediate for the synthesis of various valuable industrial products such as acetic acid, acetate esters, and pentaerythritol [1,2]. The non-oxidative dehydrogenation of ethanol to acetaldehyde and hydrogen has long been considered as an important method to produce acetaldehyde [3,4]. Although supported Cu nanoparticles (NPs) are the commercial catalysts used in the ethanol dehydrogenation reaction, the catalytic activity of Cu has been found to decrease rapidly even during the first hour of the reaction, due to sintering of Cu NPs at elevated temperatures [4–8]. Therefore, it is desirable to develop new catalysts that are highly active and selective, with improved catalyst stability for the ethanol dehydrogenation reaction. Clearly, the development of Cu-based alloys possessing these properties is the first consideration.

Similar to Cu, Au- based catalysts have also been extensively studied for the non-oxidative ethanol dehydrogenation [3,9–12]. For example, it has been reported that atomically dispersed Au species supported on $ZnZrO_x$ composite oxides are highly active and selective for the dehydrogenation of ethanol to acetaldehyde and hydrogen at low temperatures (< 200 °C), even in the presence of water [9]. The isolated Au-O_x species seem to play the key role in the activation of ethanol and its subsequent dehydrogenation reaction. In earlier work, however, it had been reported that the size of gold is the crucial factor, as supported Au NPs of certain particle size were found to exhibit good activity and selectivity for ethanol dehydrogenation [3].

It is generally agreed that the non-oxidative alcohol dehydrogenation on supported catalysts involves the following steps: 1) O—H bond scission, 2) C—H bond scission, and 3) H_2 recombination and desorption [3,12–14]. Despite extensive studies, there is no consensus or direct evidence of the rate determining step of alcohol dehydrogenation. Some studies have suggested that the C—H bond scission is the rate determining step [3,12,13], while others proposed that O—H bond scission or hydrogen recombination and desorption determine the reaction rate [15–17]. Obviously, identification of the rate determining step in ethanol dehydrogenation is crucial for better design of new catalysts that exhibit optimal catalytic activity and stability in the reaction.

The design of atomically dispersed supported metal catalysts on various supports has attracted increasing attention in recent years [18–21]. Extending to metal matrices, novel single-atom alloys (SAAs) that are composed of singly dispersed active metal atoms embedded into a less active host metal, have been prepared and reported to exhibit

* Corresponding author.
E-mail address: maria.flytzani-stephanopoulos@tufts.edu (M. Flytzani-Stephanopoulos).

https://doi.org/10.1016/j.apcatb.2017.12.059
Received 9 June 2017; Received in revised form 20 December 2017; Accepted 22 December 2017
Available online 29 December 2017
0926-3373/

unique catalytic activity for a variety of hydrogenation and dehydrogenation reactions [22–29]. For example, Pd_1Cu SAAs were reported to have an order of magnitude higher activity for the phenylacetylene hydrogenation compared to monometallic Cu, while maintaining a high selectivity to styrene [24]. Pt_1Cu SAAs are highly active and selective for 1,3 butadiene hydrogenation to butene under mild conditions [25]. The unique catalytic activities of Pd_1Cu and Pt_1Cu SAAs in various hydrogenation and dehydrogenation reactions are attributed to the presence of isolated Pd and Pt atoms that act as entrance and exit routes for hydrogen dissociation and re-combination. Spillover of H atoms onto the Cu surfaces contributes to the increased activity of the latter. In the hydrogenation reactions, a truly bifunctional catalyst was demonstrated [30].

In a previous study, we have reported that adding a small amount of Ni in Cu increases the catalytic activity of Cu in the dehydrogenation of ethanol to acetaldehyde, and improves the stability of these catalysts [29]. Our characterization data showed that Ni is atomically dispersed in Cu, and such highly dispersed Ni species in Cu may not only stabilize the Cu catalysts, but can also have a direct effect on the reaction mechanism of ethanol dehydrogenation [29]. Furthermore, Pt_1Cu SAAs have been reported to catalyze the dehydrogenation of methanol to formaldehyde and H_2 in the presence of water as co-catalyst [27], as well as the dehydrogenation of formic acid [28]. C—H bond cleavage is an important step in these dehydrogenation reactions, and thus certain types of SAAs could exhibit good activity in the activation of C—H bonds. Using more than one carbon atom, as in ethanol, the selective C—H bond activation can be studied, that is in the absence of undesired C—C bond scission that leads to the formation of CO and CO_2. The selective dehydrogenation of ethanol is thus a suitable reaction to evaluate the catalyst activity and selectivity in the activation of C—H bonds. The identification of the O—H or C—H bond activation as the rate limiting step in the dehydrogenation of alcohols may also be addressed with ethanol.

In the present study, we examined the catalytic activity of Pt_1Cu and Pd_1Cu SAAs, and NiCu SAA alloys in the ethanol dehydrogenation reaction. Unlike Ni, our data show that the presence of single Pd or Pt atoms in Cu have negligible promotion effect on the activity of Cu for this reaction. *In-situ* DRIFTS data indicates that the silica support facilitates the O—H bond cleavage of ethanol to form ethoxy intermediates over all the supported alloy catalysts. However, these remain unreactive up to 250 °C for the Cu/SiO_2 monometallic nanoparticles, while in the NiCu SAA, acetaldehyde is formed at much lower temperatures, below 150 °C. Thus, Ni facilitates the C—H bond scission of ethanol, lowering the apparent activation energy of ethanol dehydrogenation. On the other hand, Pt and Pd atoms are not as effective. More importantly, this study provides the direct evidence that the C—H bond activation is the rate determining step in ethanol dehydrogenation.

2. Experimental

2.1. Catalyst preparation

Pd_1Cu and Pt_1Cu SAAs were prepared by the galvanic replacement method [24,25], whereas NiCu SAA alloys were synthesized by a modified electroless galvanic deposition method [29]. Two types of NiCu alloys were prepared, namely silica supported NiCu NPs and unsupported nanoporous NiCu alloys (np-NiCu). The preparation procedures for these two types of NiCu alloys have been described in detail in a recent publication [29]. A summary is given below. Firstly, metallic Cu NPs were prepared using a wet chemistry approach [24,27]. Accordingly, a 0.1 M solution of ascorbic acid was added to a mixed aqueous solution of $Cu(NO_3)_2$ and polyvinylpyrrolidone (PVP) (200:1 molar ratio of Cu to PVP), under nitrogen bubbling and continuous stirring at RT. 0.1 M $NaBH_4$ was added drop-wise into the solution, upon which the solution turned to an opaque brown suspension. Subsequently, pre-activated fumed silica was suspended in deionized water under constant stirring, and added drop-wise to the colloidal solution. The solution was then kept under nitrogen protection and constant stirring for 30 min, and the solid was collected through filtering and washing with deionized water several times, followed by drying in vacuum for 12 h and calcination in air to 350 °C for 4 h. The product was reduced in pure hydrogen at 350 °C for 3 h to obtain supported metallic Cu NPs. The typical Cu loading is 8 wt% as determined by inductively coupled plasma (ICP) elemental analysis.

A modified electroless galvanic deposition method was developed to deposit atoms of Ni to Cu, based on the following redox reaction:

$$2Cu + 2OH^- + Ni^{2+} = Cu_2O + Ni + H_2O,\ \Delta E^0 = +0.103\ V \quad (1)$$

Accordingly, Ni atoms can be deposited on the surface of Cu_2O, which is spontaneous formed by the oxidation of the Cu metal in the presence of OH^- (alkaline solution). The deposition procedure was as follows: 0.01 M NaOH was added drop-wise to the $Ni(NO_3)_2{\cdot}6H_2O$ solution under nitrogen protection and continuous stirring to reach a pH value of 10.83. Then, a certain amount of pre-reduced Cu/SiO_2 NPs was added into the solution, and was held for 1 h under nitrogen protection and continuous stirring. The suspension was then filtered and washed with deionized water several times, followed by vacuum drying at 70 °C overnight. The product was further reduced in pure hydrogen at 400 °C for 3 h. The typical atomic ratio of Ni in Cu ranges from 1:100 to 1:1000, as determined by ICP.

Unsupported nanoporous Cu material was prepared through the sacrificial support method [31]. Firstly, pre-reduced Cu/SiO_2 was dispersed in an 8 M KOH solution under continuous stirring at room temperature for 36 h. The silica was removed during that step, and the remaining solid was filtered and washed with deionized water until the pH = 7, followed by vacuum drying at 70 °C overnight. Reducing in pure hydrogen at 350 °C for 3 h was used to obtain unsupported nanoporous Cu (np-Cu). Ni was added onto the np-Cu using the same electroless galvanic deposition method discussed above. After Ni deposition, the solid was reduced in pure hydrogen at 400 °C for 3 h to obtain the final product, np-NiCu. The atomic ratio of Ni in Cu in np-NiCu materials was determined by ICP.

The galvanic replacement method was used to deposit Pt and Pd into the Cu surface. The addition of Pt atoms to Cu NPs was performed in an aqueous solution at 80 °C with nitrogen protection and continuous stirring. Certain amounts of $H_2PtCl_6{\cdot}xH_2O$ were added to a suspension of silica supported Cu NPs in an aqueous solution containing 2 mM HCl. After 20 min reaction, the obtained material was filtered and washed with deionized water several times at 60 °C, and then dried in vacuum at 60 °C overnight. The solid was then reduced in hydrogen (10% balanced in He) at 350 °C for 1 h to obtain silica supported Pt_1Cu SAAs. To deposit Pd atoms into the Cu surface, desired amounts of Pd $(NO_3)_2{\cdot}6H_2O$ were added to a suspension of Cu/SiO_2 NPs at room temperature. The reaction was held for 1 h under nitrogen protection and constant stirring, and then the solid was filtered and washed with deionized water several times. The obtained product was dried in vacuum at 60 °C overnight, and was reduced in hydrogen (10% balanced in He) at 350 °C for 1 h to obtain Pd_1Cu SAAs. The Pt and Pd loadings were measured by ICP.

2.2. Characterization methods

X-ray powder diffraction (XRD) patterns were collected on a PANalytical X'Pert Pro instrument using nickel-filtered Cu Kα radiation (λ = 1.54056 Å). The measurements were taken at 45 kV and 40 mA in a continuous mode. Data was collected for 2θ between 25° and 80°. Diffuse reflectance infrared Fourier transform spectroscopy (DRIFTS) measurements were conducted on a Thermo Scientific Nicolet iS50 FTIR Spectrometer and a Praying Mantis high temperature reaction chamber. Typically, samples were reduced *in situ* with 10% H_2/He at a

flow rate of 10 mL/min at 350 °C for 1 h.

In-situ X-ray Absorption Near Edge Structure (XANES), and Extended X-Ray Absorption Fine Structure (EXAFS) measurements were performed at beamline 12-BM at Argonne National Laboratory. XANES and EXAFS data of NiCu alloys at the Ni K-edge and Cu K-edge in fluorescence mode were collected. XANES and EXAFS data of Ni metal foil and Cu metal foil were also collected in the reference mode for X-ray energy calibration and data alignment. Approximately 7 consecutive scans were collected for each sample to improve the signal-to-noise ratio. EXAFS data processing and analysis were performed using the IFEFFIT package.

The ethanol dehydrogenation activities of Pt_1Cu, Pd_1Cu, and NiCu alloys were evaluated in a fixed-bed flow reactor at atmospheric pressure. Certain amounts of sample was loaded into a U-shaped quartz reactor tube between two layers of quartz sand and packed in between two quartz wool plugs. The reactor was heated in a furnace equipped with a temperature controller. The temperature of the catalyst was measured with a K-type thermocouple reaching the top of the catalyst bed. Prior to testing, all catalysts were reduced under a flow of H_2 (10% in argon) with a flow rate of 10 mL/min at 350 °C for 1 h. The reaction gas composition was 5.6% ethanol balanced in He, through a bubbler system, using a flow rate of 10 mL/min. The effluent gas was monitored online by a residual gas analyzer (SRS RGA 200). Ethanol, acetaldehyde, ethyl acetate, H_2, CO, CO_2, and C_2H_4 were monitored by m/z = 31, 29, 61, 2, 28, 44, and 27, respectively. In the case of acetaldehyde, the contribution from the ethanol fragment was subtracted from the original m/z = 29 signal prior to further processing.

3. Results and discussion

XRD patterns of unsupported np-Cu, np-$Ni_{0.01}Cu$, and np-$Ni_{0.01}Cu$ after ethanol dehydrogenation at 250 °C for 8 h are shown in Fig. 1. The XRD pattern of np-Cu is dominated by diffraction peaks related to the (111), (200) and (220) lattice planes of metallic Cu.[32] Similarly, the XRD patterns of np-NiCu before and after reaction are also dominated by the (111), (200) and (220) lattice planes of metallic Cu, indicating that the nanoporous materials prepared by the sacrificial support method are not amorphous but are well-crystallized. Furthermore, no XRD peaks related to Ni are observed, although the Ni concentration in np-$Ni_{0.01}Cu$ is probably too low to exclude the formation of separate Ni phase based on the XRD data alone. Moreover, the XRD patterns of np-NiCu after the reaction were preserved, and no separate Ni phases were formed, at least not detectable by XRD at these small Ni contents.

In addition, for unsupported nanoporous Cu materials, the diffraction peak related to Cu_2O phase is not present, which was observed in the case of supported Cu NPs [29]. Such difference might be due to the very small surface area of np-Cu (8.7 m^2/g), compared to Cu NPs (48 m^2/g). These surface area values were obtained through the methods described in a recent publication [29]. Also, as the oxidation is much easier to occur on Cu defect sites, *i.e.* under-coordinated Cu atoms [33], the concentration of under-coordinated Cu atoms in nanoporous Cu materials is probably much lower than that in supported Cu NPs. The total pore volume of np-Cu is determined at 0.057 cm^3/g. There are no significant changes of the surface area and total pore volume of nanoporous Cu materials after the deposition of a small amount of Ni.

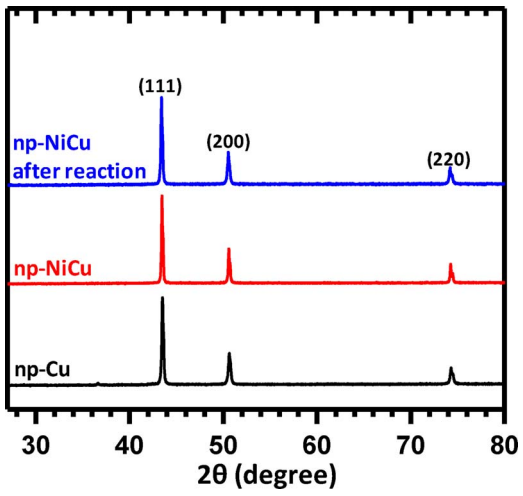

Fig. 1. XRD patterns of unsupported np-Cu, unsupported np-$Ni_{0.01}Cu$, and unsupported np-$Ni_{0.01}Cu$ after the ethanol dehydrogenation reaction at 250 °C for 8 h.

High-resolution transmission electron microscope (HRTEM) images and scanning electron microscope (SEM) images of various NiCu SAA alloys and Pt_1Cu SAAs were shown in our recent publications [27,29], and therefore are not shown here. These images clearly show the crystalline nature of the supported nanoparticle catalysts and unsupported nanoporous catalysts. Moreover, the STEM imaging of Pt_1Cu SAAs also supports the formation of isolated Pt atoms in the surface of Cu [27].

The photoemission features of Ni 2p and Cu 2p were obtained for np-$Ni_{0.01}Cu$ before reduction, after reduction, and after ethanol dehydrogenation. The Ni/Cu surface atomic ratio before reduction is 0.12 and decreases to 0.06 after reduction and after ethanol dehydrogenation, indicating that after reduction Ni atoms partially diffuse to the subsurface, and remain in the subsurface during ethanol dehydrogenation. In addition, Ni 2p spectra also indicate that before reduction Ni^{2+} is the dominant species, while after reduction, the portion of metallic Ni significantly grows. The remaining of Ni^{2+} after reduction is possibly due to the re-oxidation of Ni^0 after exposing the sample to air after the reduction. Furthermore, we also tried XPS measurements of $Ni_{0.01}Cu$ NPs, however the low Ni concentration in the supported catalyst does not yield a measurable signal of Ni [29].

The catalytic performance of Pd_1Cu, Pt_1Cu, and NiCu alloys in the ethanol dehydrogenation reaction was examined by measuring the reaction kinetics in steady-state conditions. In all measurements, the conversion of ethanol was kept below 15%. No CO, C_2H_4, or CO_2 were detected in these measurements, indicating nearly 100% selectivity to acetaldehyde up to 350 °C. Apparently, these catalysts do not catalyze C—C bond scission of ethanol. Table 1 lists the calculated apparent activation energies of silica- supported monometallic Cu NPs, np-Cu, $Pd_{0.01}Cu$ NPs, $Pt_{0.01}Cu$ NPs, $Ni_{0.001}Cu$ NPs, $Ni_{0.01}Cu$ NPs, and np-$Ni_{0.01}Cu$. These apparent activation energies are calculated from their corresponding measured reaction rates. Fig. 2 shows the Arrhenius-type plots of the H_2 formation rate on monometallic Cu NPs, $Pd_{0.01}Cu$ NPs, $Pt_{0.01}Cu$ NPs, and $Ni_{0.01}Cu$ NPs. For clarity, Arrhenius-type plots of other samples are not included in Fig. 2. The H_2 formation rates are normalized by the Cu surface area for each catalyst. For nanoparticle based catalysts, the surface area of Cu is 48 m^2/g, while for unsupported nanoporous materials, the surface area of Cu is 8.7 m^2/g [29]. The calculated carbon mass balances in all cases are close to 100%.

As shown in Table 1, the apparent activation energies for monometallic Cu NPs and for np-Cu are similar, 70 ± 5 kJ/mol and

Table 1
Apparent activation energies of the ethanol dehydrogenation reaction on monometallic Cu catalysts, $Pd_{0.01}Cu$ NPs, $Pt_{0.01}Cu$ NPs, and various NiCu SAA alloys.

Samples	E_a (kJ/mol)
Cu NPs	70 ± 5
np-Cu	73 ± 6
$Pd_{0.01}Cu$ NPs	69 ± 4
$Pt_{0.01}Cu$ NPs	63 ± 6
$Ni_{0.001}Cu$ NPs	49 ± 4
$Ni_{0.01}Cu$ NPs	47 ± 2
np-$Ni_{0.01}Cu$	45 ± 4

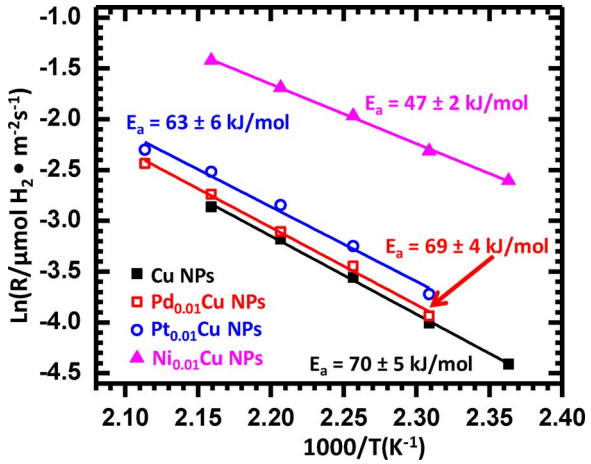

Fig. 2. Arrhenius-type plots of the reaction rate in ethanol dehydrogenation, normalized by the surface area of Cu over monometallic Cu NPs, $Pd_{0.01}Cu$ NPs, $Pt_{0.01}Cu$ NPs, and $Ni_{0.01}Cu$ NPs.

73 ± 6 kJ/mol, respectively. For the alloys, Pt has more of an effect than Pd, but the effect of both is much less than that of Ni, with $Ni_{0.001}Cu$ NPs, $Ni_{0.01}Cu$ NPs, and np-$Ni_{0.01}Cu$ (SSM) showing E_a = 49 ± 4 kJ/mol, 47 ± 2 kJ/mol, and 45 ± 4 kJ/mol, respectively. Clearly, adding a small amount of Ni in Cu dramatically decreases the activation barrier of ethanol dehydrogenation, in other words it improves the reactivity of Cu.

Fig. 3 shows the normalized Ni *in operando* XANES spectra of various NiCu alloys under reaction conditions, as well as Ni standards. XANES data of NiCu alloys were collected in fluorescence mode, while the data of Ni standards were collected in the transmission mode. XANES data for $Ni_{0.001}Cu$ NPs after reduction, $Ni_{0.001}Cu$ NPs during ethanol dehydrogenation reaction, $Ni_{0.01}Cu$ NPs after reduction, $Ni_{0.01}Cu$ NPs during ethanol dehydrogenation reaction, as well as Ni foil and NiO standards are shown in Fig. 3a. For better comparison, *in situ* XANES data of np-$Ni_{0.001}Cu$ after reduction, $Ni_{0.001}Cu$ NPs after reduction, $Ni_{0.01}Cu$ NPs after reduction, and Ni foil, as well as the linear combination fitting of $Ni_{0.01}Cu$ NPs after reduction are shown in Fig. 3b. For the spectra after reduction, samples were pre-reduced in 4% H_2 (balanced in He) at 350 °C for 1 h and cooled down to room temperature in hydrogen atmosphere prior to collecting the data. For the spectra during reaction, samples were treated in 5.6% ethanol (balanced in He) at 250 °C for 30 min and were kept at this condition during the data acquisition.

The XANES spectra of $Ni_{0.01}Cu$ NPs in Fig. 3a clearly shows that after reduction, Ni is not in 2+ oxidation state; Ni species are neutral. This conclusion is in line with CO-DRIFTS study of the same samples [29]. Furthermore, during the ethanol dehydrogenation reaction, the XANES spectra of $Ni_{0.01}Cu$ NPs are similar to the spectra of the same sample after reduction, indicating that Ni remains neutral during ethanol dehydrogenation. Moreover, as shown in Fig. 3, the XANES spectrum of $Ni_{0.001}Cu$ NPs is very different from that of $Ni_{0.01}Cu$ NPs. A high intensity white line is present in the spectra of $Ni_{0.001}Cu$ NPs. Such high intensity while line is usually caused by the Ni-O interaction, in other words, the oxidation of Ni [34,35]. Similar to the spectra of NiO standard, the XANES spectra of oxidized Ni species do not have the pre-edge feature that is present in the Ni foil, as reported in the literature [34,36,37]. Here, however, a pre-edge feature similar to the Ni foil is clearly present in the spectra of $Ni_{0.001}Cu$ NPs, as shown in Fig. 3a. In addition, as will be discussed below, Ni—O bond is not present in the EXAFS spectra of the same sample. These observations indicate that the high intensity white line in $Ni_{0.001}Cu$ NPs is not due to the oxidation of Ni. Interestingly, similar high intensity white line of Ni has been reported before in a PtNi bimetallic system, in which highly diluted Ni atoms are atomically distributed in Pt [38]. Therefore, the high intensity white line in $Ni_{0.001}Cu$ NPs is more likely due to the presence of singly dispersed Ni atoms in Cu, that only alloy with Cu atoms. It has been reported that the Ni K edge white line intensities of NiCu bimetallic alloys continuously increase with decreasing of Ni concentrations in alloys, although such intensity increases are not significant [39]. The increase of the white line intensity was attributed to the transfer of *p* charge from Ni to Cu if Ni alloys with Cu [39]. Apparently, such *p* charge transfer might be more pronounced when Ni is singly distributed in Cu, *i.e.*, when Ni atoms only bind with Cu atoms.

Moreover, the XANES spectrum of the unsupported np-$Ni_{0.001}Cu$ resembles the spectrum of $Ni_{0.001}Cu$ NPs, indicating that Ni species in the nanoporous np-$Ni_{0.001}Cu$ also form isolated Ni atoms. In addition, during the ethanol dehydrogenation reaction, XANES spectra of $Ni_{0.001}Cu$ NPs are similar to the spectra of the same sample after reduction, suggesting that Ni remains isolated during ethanol dehydrogenation.

On the other hand, the intensity of the white line in $Ni_{0.01}Cu$ NPs is significantly smaller, and the XANES spectra somehow resemble the Ni foil, indicating the presence of Ni-Ni interaction. Interestingly, as shown in Fig. 3b, the XANES spectrum of $Ni_{0.01}Cu$ NPs can be fitted by a linear combination of the spectra of $Ni_{0.001}Cu$ (35%) and Ni foil (65%). As found by CO-DRIFTS, for $Ni_{0.01}Cu$ NPs the presence of large Ni NPs can be excluded.[29] Ni is therefore likely present as both single atoms (35%) and sub-nano clusters (65%) in $Ni_{0.01}Cu$ NPs.

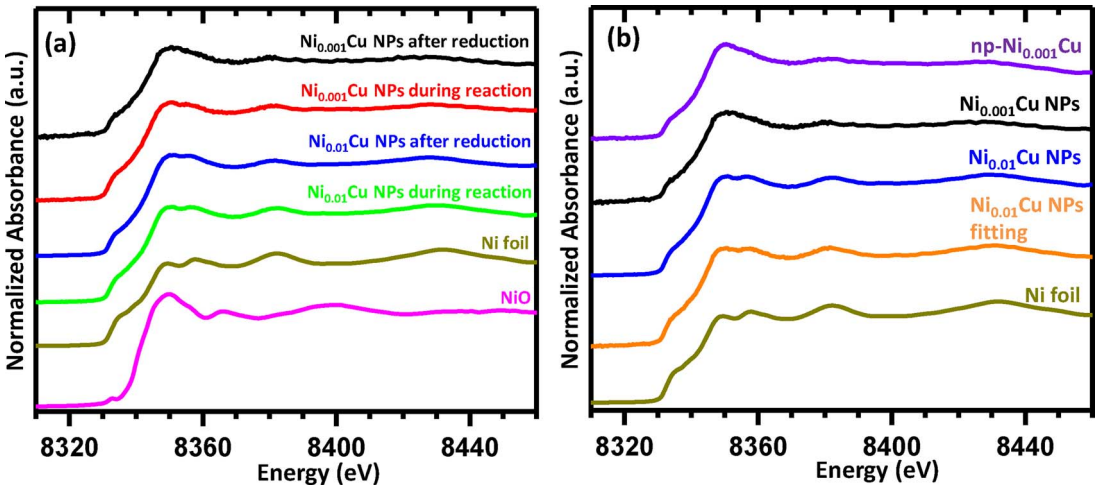

Fig. 3. Normalized Ni XANES spectra of various NiCu alloys after reduction and during the ethanol dehydrogenation reaction, as well as Ni foil and NiO standards. 3(a) shows the spectra after reduction and during reaction, and 3(b) shows the spectra after reduction and the fitting of $Ni_{0.01}Cu$ NPs after reduction. See text for detailed description.

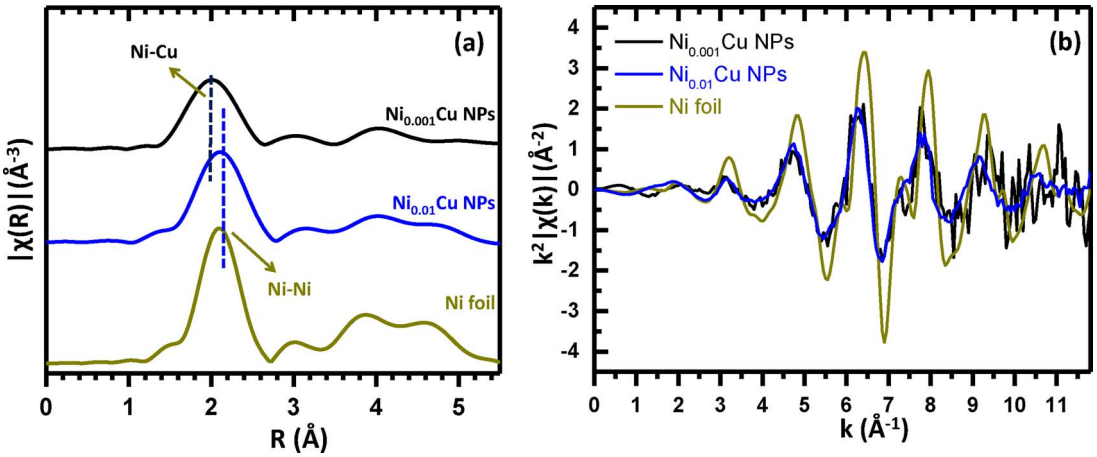

Fig. 4. Ni K-edge EXAFS data of $Ni_{0.001}Cu$ NPs after reduction, $Ni_{0.01}Cu$ NPs after reduction, and Ni foil standard. 4(a) shows the R space spectra, and 4(b) shows the k space spectra. The samples were pre-reduced *in-situ* with 4% H_2 (balanced in He) at 350 °C for 1 h prior to collecting the spectra.

Table 2
Quantitative analyses for Ni-Ni and Ni-Cu contributions to the EXAFS data.

Sample	Shell	CN[a]	R (Å)[b]	σ^2(Å^2)[c]
$Ni_{0.001}Cu$	Ni-Ni	0	–	–
	Ni-Cu	8.31 ± 1.5	2.40 ± 0.07	0.008
Ni foil	Ni-Ni	12	2.49 ± 0.01	0.007

[a] CN, coordination number.
[b] R, distance between absorber and backscattered atoms.
[c] σ^2, EXAFS Debye-Waller factor for individual shells.

EXAFS data at the Ni K-edge of the silica supported $Ni_{0.001}Cu$ NPs after reduction and $Ni_{0.01}Cu$ NPs after reduction are shown in Fig. 4. The samples were pre-reduced in-situ with 4% H_2 (balance He) at 350 °C for 1 h prior to collecting the EXAFS data in the fluorescence mode at room temperature. The Ni K-edge R-space EXAFS spectra clearly shows that the first coordination shell of $Ni_{0.001}Cu$ NPs and $Ni_{0.01}Cu$ NPs are at different positions. As the majority of Ni atoms in $Ni_{0.001}Cu$ NPs are isolated and only bind with Cu atoms, the EXAFS spectra of $Ni_{0.001}Cu$ were therefore fitted with a single Ni-Cu scattering path. The Ni-Cu coordination number and bond length derived from the fit are shown in Table 2. As estimated from the XANES spectra, Ni species in $Ni_{0.01}Cu$ consist of both single atoms (35%) and sub-nano clusters (65%), the EXAFS spectra of $Ni_{0.01}Cu$ might be able to be fitted with a combination of Ni-Cu scattering path and Ni-Ni scattering path. However, the extremely close length of Ni-Cu and Ni-Ni scattering path makes it almost impossible to differentiate Ni-Cu and Ni-Ni contribution in the EXAFS spectra of $Ni_{0.01}Cu$. On the other hand, the EXAFS spectra also clearly show that the Ni—O bond is not present in either sample.

It is generally agreed that the bond length of Ni—Cu bond should be between the length of Ni—Ni and Cu—Cu bonds.[40] However, we found that when Ni atoms are singly dispersed in Cu, the Ni—Cu bond length (2.40 Å) is smaller than either the Ni-Ni bond (2.49 Å) or the Cu—Cu bond (2.55 Å). In catalysis measurements, we also found that adding such a small amount of Ni to Cu forming isolated Ni atoms can significantly improve the reactivity of Cu in ethanol dehydrogenation. This observation suggests that isolated Ni atoms are likely present in Cu surface forming highly under-coordinated Ni atoms rather than bulk alloy. In fact, the low coordination number of Ni (8.31 ± 1.5) in $Ni_{0.001}Cu$, as well as the relatively small Ni—Cu bond length also support the formation of highly under-coordinated Ni atoms on the Cu surface. Furthermore, it has been reported that charge transfer can significantly affect the bond length of metals [41,42]. Therefore, it is possible that the Ni—Cu bond length is also influenced by the enhanced charge transfer between isolated Ni atoms and Cu in $Ni_{0.001}Cu$.

The XAS data at the Cu K-edge of $Ni_{0.001}Cu$ NPs after reduction, $Ni_{0.01}Cu$ NPs after reduction, and Cu NPs after reduction, as well as the Cu foil standard are shown in Fig. 5. The normalized Cu XANES spectra in Fig. 5a clearly shows that after reduction, Cu species in these samples are in the metallic state. This conclusion also agrees to the k space Cu EXAFS spectra in Fig. 5b and the R space Cu EXAFS spectra in Fig. 5c. The Cu-Cu coordination number and bond length derived from the fitting of Cu EXAFS data are listed in Table 3. The Cu-Cu coordination number and bond length of these samples clearly shows that adding a small amount of Ni to Cu does not change the overall bonding environment of Cu. Likely, the local charge transfer between atomically dispersed Ni atoms and Cu atoms plays a crucial role in improving the stability of Cu materials against sintering at high temperatures.

For the other two minority metals (Pt, Pd) in Cu, studied here, we

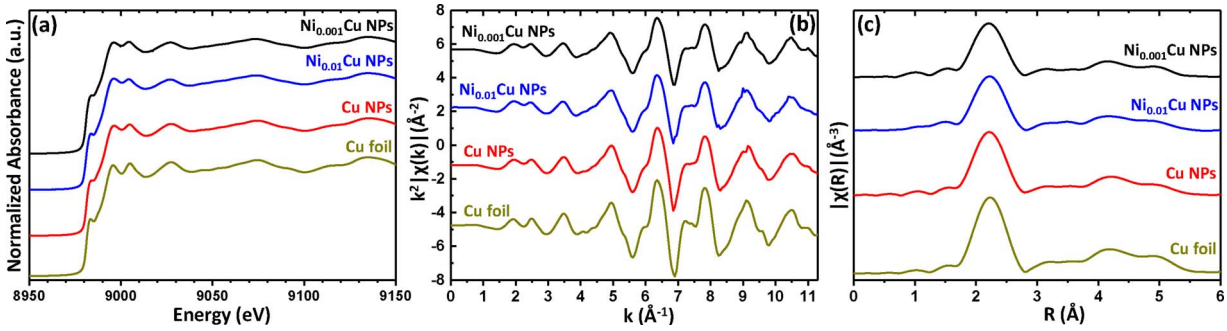

Fig. 5. Cu K-edge XAS data of $Ni_{0.001}Cu$ NPs after reduction, $Ni_{0.01}Cu$ NPs after reduction, Cu NPs after reduction, and Cu foil standard. 5(a) shows the normalized Cu XANES spectra; 5(b) shows the k space Cu EXAFS spectra; 5(c) shows the R space Cu EXAFS spectra. The samples were pre-reduced in-situ with 4% H_2 (balanced in He) at 350 °C for 1 h prior to collecting the spectra. The Cu-Cu coordination number and bond length derived from the fitting of Cu EXAFS data are shown in Table 3.

Table 3
Quantitative analyses for Cu-Cu contributions to the EXAFS data in Fig. 5.

Sample	Shell	CN[a]	R (Å)[b]	σ^2(Å^2)[c]
$Ni_{0.001}Cu$	Cu-Cu	9.8 ± 0.9	2.55 ± 0.02	0.009
$Ni_{0.01}Cu$	Cu-Cu	10.1 ± 1.0	2.55 ± 0.02	0.009
Cu NPs	Cu-Cu	10.5 ± 0.8	2.54 ± 0.02	0.008
Cu foil	Cu-Cu	12	2.54 ± 0.01	0.007

[a] CN, coordination number.
[b] R, distance between absorber and backscattered atoms.
[c] σ^2, EXAFS Debye-Waller factor for individual shells.

note that $Pt_{0.01}Cu$ NPs have been well characterized by various techniques, and the single atom distribution of Pt in the Cu surface has been confirmed [26,27]. Moreover, alumina supported $Pd_{0.01}Cu$ NPs have been prepared by the same galvanic replacement method as silica supported $Pd_{0.01}Cu$ NPs, and various characterizations show that the Pd atoms are singly distributed in Cu therein [24]. It is expected that Pd atoms are also singly dispersed in the Cu surface on the silica supported $Pd_{0.01}Cu$ NPs used here. Overall, in $Ni_{0.001}Cu$ NPs, $Pt_{0.01}Cu$ NPs, and $Pd_{0.01}Cu$ NPs, the minority metals are all present as single atoms in Cu.

It has been demonstrated before that single Pd and Pt atoms in Cu activate and dissociate hydrogen, the H atoms spilling over onto the bare Cu surface where they are weakly bound and effective for hydrogenation reactions [22]. Isolated Pd and Pt atoms can also act as the recombination and desorption sites for hydrogen, in other words the presence of isolated Pd and Pt atoms in Cu lowers the reaction barrier for hydrogen atom recombination and desorption. Note that hydrogen atom recombination and desorption is an important step in ethanol dehydrogenation. Obviously, if this is the rate determining step, adding single Pd or Pt atoms in Cu should increase the reaction rate of Cu in ethanol dehydrogenation by lowering the barrier of hydrogen recombination and desorption. However, Fig. 2 and Table 1 clearly show that adding a small amount of isolated Pt or Pd atoms in Cu does not decrease appreciably the apparent activation energy of the reaction on Cu. Hence, hydrogen recombination and desorption is not the rate determining step in ethanol dehydrogenation.

In recent studies, it has been found that single Pt or Pd atoms in Cu can lower the barrier for O—H bond cleavage of formic acid and methanol [23,27,28]. Adding a small amount of Pt or Pd in Cu can likely also lower the activation barrier for O—H bond scission of ethanol. If the O—H bond scission is the rate determining step in this reaction, adding a small amount of Pt or Pd in Cu will lower the apparent activation energy in ethanol dehydrogenation, which was not observed in our catalysis measurements. Therefore, it is unlikely that the O—H bond scission is the rate determining step. Our catalysis data thus suggest that the C—H bond scission is the rate determining step in ethanol dehydrogenation. As shown in Fig. 2 and Table 1, adding a small amount of Ni in Cu significantly decreases the apparent activation energy of ethanol dehydrogenation. The promotional effect of Ni is likely due to the participation of Ni atoms in the C—H bond scission of ethanol. To further identify the rate determining step and to understand the role of Ni in ethanol dehydrogenation, *in-situ* FTIR reaction studies were conducted in the DRIFTS mode over various catalysts.

DRIFT spectra of the silica powder under various conditions are shown in Fig. 6. Cu-free silica powder was first pre-treated with He at a flow rate of 10 mL/min at RT for 10 min, followed by collecting DRIFT spectra in He at RT (He RT). The sample was further treated in He at 150 °C for 30 min, and DRIFT spectra were recorded in He at 150 °C (He 150 °C). Then the sample was cooled down to RT in He, and ethanol vapor was introduced (5.6% balanced in He) at RT for 10 min, through a bubbler system, using a flow rate of 10 mL/min. Thereafter, the flow was switched to pure He for 3 min to remove gas phase ethanol. Then He flow was stopped, and the spectra were collected in RT (EtOH RT). The sample was heated to 150 °C in He and ethanol vapor was passed over the catalyst surface at 150 °C for 10 min, followed by He purge at 150 °C for 3 min. After this, the He flow was stopped, and DRIFT spectra were collected at 150 °C (EtOH 150 °C). A similar procedure was also used to collect the spectra at 250 °C after ethanol introduction (EtOH 250 °C). For Fig. 6a, background spectra were collected on KBr powder at corresponding temperatures under the He flow; for Fig. 6b, background spectra were obtained on silica powder at corresponding temperatures under He, except the spectrum of He 150 °C, where the background spectrum was collected under He at RT.

The DRIFT spectra in the O—H stretching regime are shown in Fig. 6a, while Fig. 6b shows the spectra in the C—H stretching regime. In Fig. 6a, the spectrum of He RT shows a very sharp band at 3744 cm^{-1} and a rather weak feature centered at approximately 3310 cm^{-1}. The sharp band at 3744 cm^{-1} is the characteristic peak of isolated silanol groups [13,43], whereas the feature centered at 3310 cm^{-1} is attributed to the O—H stretch of adsorbed water on silica. [44] After heating to 150 °C in He, the feature centered at 3310 cm^{-1} disappears, indicating the removal of water molecules from the silica surface. The persistence of 3744 cm^{-1} peak in the spectrum of He 150 °C shows the dominance of isolated surface silanol groups. Moreover, after ethanol introduction at RT, the 3744 cm^{-1} peak completely disappears, and a rather broad feature centered at approximately 3380 cm^{-1} appears. This broad band centered at 3380 cm^{-1} has been assigned to the O—H stretch of hydrogen bonded Si—OH groups [13,43,45]. Fig. 6b also shows that after ethanol introduction at RT, several peaks in the C—H stretching regime appear, which are assigned to C—H stretches of adsorbed ethanol molecules.[13,43] The two dominant peaks are at 2980 cm^{-1} (CH_3 asymmetric stretching), and 2903 cm^{-1} (CH_2 asymmetric stretching).[13,33] Combining these observations in the O—H stretching and C—H stretching regimes suggests that adsorbed ethanol molecules are likely hydrogen bonded to the silica surface through silanol groups, as shown in the inset of Fig. 6a.

The spectra taken at 150 °C in Fig. 6a clearly shows the reappearance of the characteristic peak of isolated silanol groups at 3744 cm^{-1}, and decrease of the peak intensity at 3380 cm^{-1}. This suggests that most of the ethanol molecules desorb from the surface, while some ethanol may still remain on the surface after evacuation at higher temperatures. Interestingly, Fig. 6b also shows that at 150 °C and 250 °C, a new peak at 2858 cm^{-1} is developed. This peak has been assigned to the C—H stretching band of adsorbed ethoxy species (CH_2 symmetric stretching) [43,46]. Thus, the DRIFT spectra in Fig. 6 clearly indicate that silica support is active for the O—H bond scission of ethanol to form ethoxy species. However, the formed ethoxy species cannot be further dehydrogenated to acetaldehyde through C—H bond cleavage, as no IR peaks related to acetaldehyde were observed up to 400 °C, which is consistent with the catalysis measurements.

Fig. 7 shows the DRIFT spectra of silica supported Cu NPs after exposure to ethanol at different temperatures. The spectra in the C—H stretching regime are shown in Fig. 7a, while Fig. 7b shows the spectra in the C—O stretching regime. The sample was first pre-reduced with 10% H_2/He at a flow rate of 10 mL/min at 350 °C for 1 h, followed by cooling down to RT in H_2. The flow was then switched to He, and ethanol vapor was introduced (5.6% balanced in He) at RT for 10 min using a flow rate of 10 mL/min, followed by He purge for 3 min at RT. Then the He flow was stopped, and the spectra were collected at RT (EtOH RT). For the spectra collected at other temperatures, ethanol vapor was introduced at certain temperature for 10 min, followed by He purge for 3 min at this temperature. Then the He flow was stopped, and the spectra were collected at the same temperature. A reference spectrum obtained on bare silica support at corresponding temperatures under the He flow was subtracted from each spectrum shown in Fig. 7.

It is noteworthy that for the spectra in the O—H stretching regime, the presence of the sharp band at 3744 cm^{-1}, as well as the disappearance of this band after ethanol introduction at RT, and the reappearance after heating were also observed (not shown here). This observation indicates the presence of isolated silanol groups on silica support and adsorbed ethanol molecules are hydrogen bonded to silica

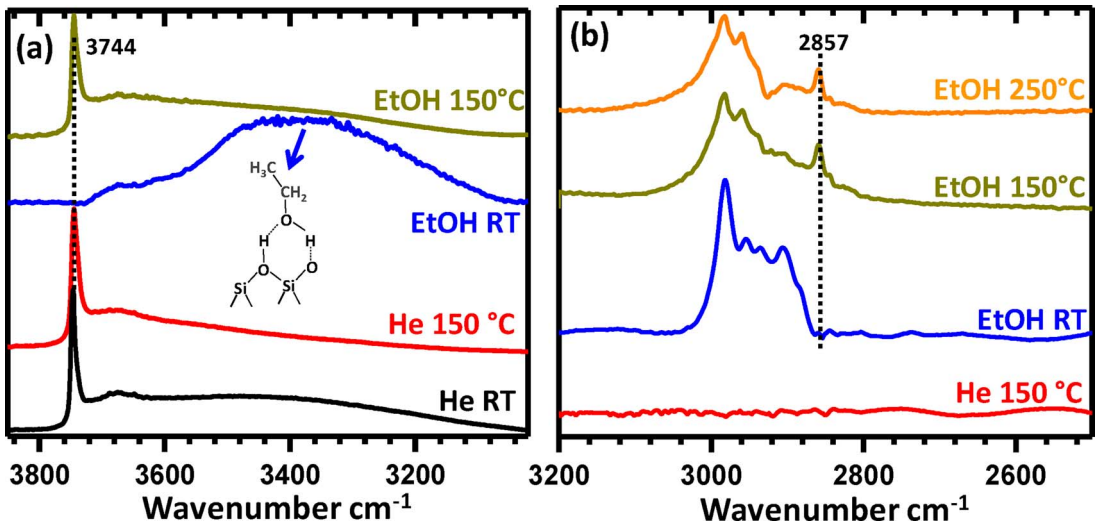

Fig. 6. DRIFT spectra of the silica support under various conditions. (a): spectra in the O—H stretching regime; (b): spectra in the C—H stretching regime. See text for detailed description.

support through silanol groups. The RT spectrum in Fig. 7a clearly shows several features related to C—H stretching bands of adsorbed ethanol. Interestingly, this spectrum is somehow different to the corresponding spectrum in Fig. 6a, which shows C—H stretching bands of adsorbed ethanol on pure silica surface. This difference might be due to the fact that on silica supported Cu NPs ethanol can bond both to bare silica support and the surface of Cu. More importantly, Fig. 7a also shows that with increase of temperature, a clear peak at 2857 cm^{-1} is developed, indicating the formation of ethoxy species. A new peak developed at 2956 cm^{-1} is also present, particularly for the spectrum at 300 °C. This peak at 2956 cm^{-1} has been reported before in a study of adsorbed ethoxy species on Cu(100) surface, and was assigned to CH_3 asymmetric stretching frequency of adsorbed ethoxy on Cu surface [46]. Therefore, the development of these peaks at 2857 and 2956 cm^{-1} suggests the formation of ethoxy species, likely adsorbed on both silica support and the surface of Cu NPs. As will be demonstrated below, and in agreement with previous reports, no IR peaks related to adsorbed ethoxy species are observed on O-free metallic Cu surface after exposure to ethanol [47]. Therefore, on supported Cu NPs, ethoxy species formed on bare silica support could partially diffuse from the silica surface to the Cu surface and adsorb onto the Cu surface.

As marked in Fig. 7a, a new broad feature centered at approximately 2740 cm^{-1} also appears for the spectrum at 300 °C, although this feature is too weak to be directly visualized without magnification. This broad feature is associated with C—H stretching frequencies of acetaldehyde species [47,48]. Furthermore, the spectrum at 300 °C in Fig. 7b shows the appearance of an intense peak at 1723 cm^{-1}, which is the characteristic peak of the C=O stretching vibration of acetaldehyde [13,47]. Thus, the DRIFT spectra in Fig. 7 clearly show the formation of acetaldehyde on silica supported Cu NPs at a high temperature (300 °C).

The DRIFT spectra of silica supported $Ni_{0.01}Cu$ NPs after exposure to ethanol at various temperatures are shown in Fig. 8. The spectra in the C—H stretching regime are shown in Fig. 8a, while the spectra in the C—O stretching regime are shown in Fig. 8b. The pre-reducing procedure and the procedure to collect the spectra at various temperatures, as well as the background subtraction are the same with supported Cu NPs. For the spectra in the O—H stretching regime (not shown here), similar spectra and evolution are observed as on supported Cu NPs and pure silica powder, indicating the presence of isolated silanol groups on bare silica support and ethanol molecules are hydrogen bonded to silica support through silanol groups.

Different from supported Cu NPs, the spectra in Fig. 8a on supported $Ni_{0.01}Cu$ NPs do not show the presence of characteristic peaks of adsorbed ethoxy species at 2857 and 2956 cm^{-1} at 150 °C and above. However, a more detailed examination does show the formation of ethoxy species at low temperatures (75–125 °C), as shown in the inset of

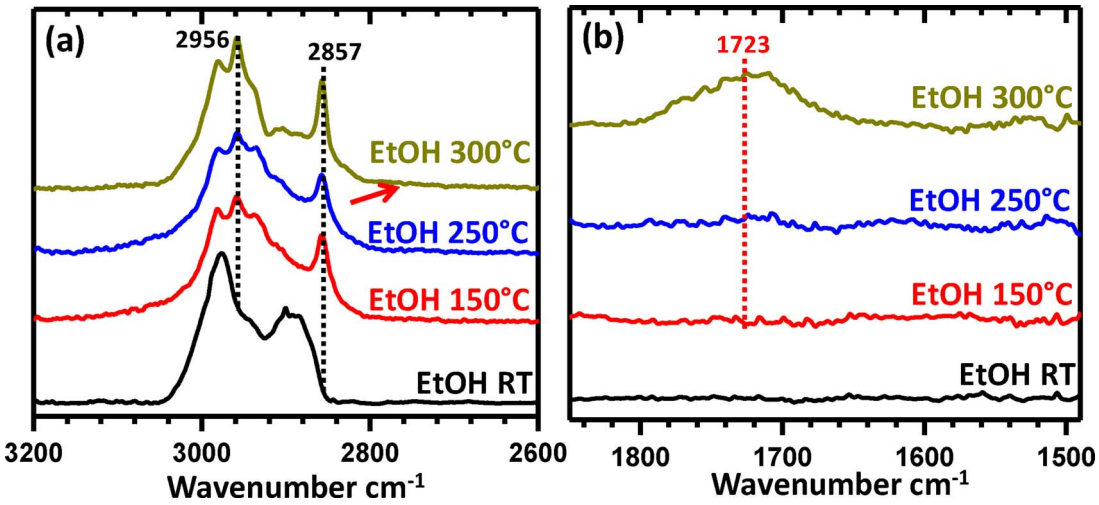

Fig. 7. DRIFT spectra of silica supported Cu NPs after exposure to ethanol at various temperatures. (a): spectra in the C—H stretching regime; (b): spectra in the C—O stretching regime. See text for details.

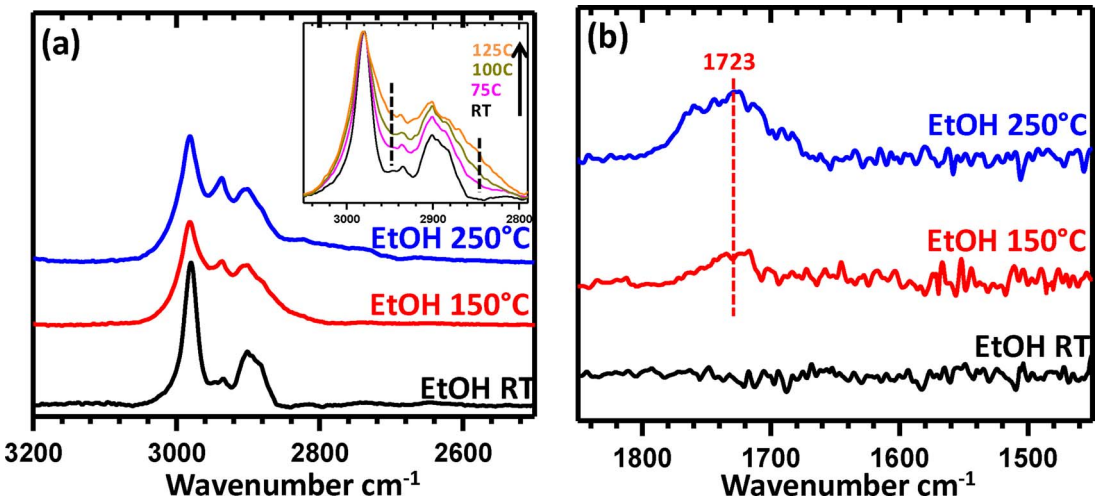

Fig. 8. DRIFT spectra of silica supported $Ni_{0.01}Cu$ NPs after exposure to ethanol at various temperatures. (a): spectra in the C—H stretching regime; (b): spectra in the C—O stretching regime. See text for details.

Fig. 8a. Apparently, the formed ethoxy species do not accumulate on the surface at 150 °C and above. Moreover, at 150 and 250 °C, the broad feature related to acetaldehyde species centered at 2740 cm^{-1} is present. Fig. 8b also clearly shows the development of the C═O stretching peak of acetaldehyde at 1723 cm^{-1}. Apparently, the formation of acetaldehyde on supported $Ni_{0.01}Cu$ NPs occurs at a much lower temperature than on Cu NPs. More importantly, the decrease of ethoxy peaks and the increase of acetaldehyde peaks suggest that the formed ethoxy species undergo further C—H bond cleavage to acetaldehyde. Clearly, Ni atoms presented in Cu must directly participate in C—H bond cleavage, and lower the required temperature for C—H bond cleavage of ethoxy species, therefore adsorbed ethoxy species do not accumulate on supported NiCu NPs at 150 °C and above.

The DRIFTS data are consistent with our catalysis measurements that adding a small amount of Ni in Cu significantly decreases the apparent activation energy of Cu in ethanol dehydrogenation. The DRIFTS data further indicate that this promotion effect is likely due to the presence of Ni atoms facilitating the C—H bond scission. They also demonstrate that although bare silica support is active for the cleavage of O—H bonds of ethanol to ethoxy, likely through the formation of surface complex of ethanol with surface silanol groups, the presence of Cu or NiCu NPs is required for the cleavage of the C—H bond of ethoxy to acetaldehyde. Such observation along with the fact that adsorbed ethoxy species continuously accumulate on Cu NPs with increasing temperature show that the activation barrier for C—H bond cleavage is much higher than that for O—H bond cleavage. Thus, the C—H bond scission is thus the likely the rate determining step in ethanol dehydrogenation.

DRIFT spectra of unsupported np-Cu materials shown in Fig. 9, further confirm this conclusion. The spectra in the O—H stretching regime, C—H stretching regime, and C—O stretching regime are shown in Fig. 9a–c respectively. The same procedure was used to pre-reduce the sample and collect the spectra at different temperatures. The background spectra for Fig. 9b and 9c were obtained on the same sample under He flow at corresponding temperatures, while for Fig. 9a, they were obtained on KBr powder under He.

Fig. 9a shows that the sharp band at 3744 cm^{-1} is not present, which is expected as silanol groups are absent on the unsupported np-Cu materials. A new peak at 3670 cm^{-1} is present at RT and 150 °C, which is assigned to the O—H stretching vibration of adsorbed ethanol on Cu [47]. The appearance of the broad feature at 2740 cm^{-1} in Fig. 9b and 1723 cm^{-1} in Fig. 9c, indicates the formation of acetaldehyde at high temperature. However, the formation of adsorbed ethoxy species is not observed on np-Cu catalysts at any temperature, as the peaks related to ethoxy at 2857 and 2956 cm^{-1} are absent. This result further confirms that surface silanol groups present on the bare silica support facilitate the cleavage of O—H bonds of ethanol. Since the same apparent activation energies of the reaction were obtained on np-Cu (73 ± 6 kJ/mol) and supported Cu NPs (70 ± 5 kJ/mol), Table 1, combining with the DRIFTS data clearly shows that O—H bond cleavage does not affect the reaction rate in ethanol dehydrogenation. In fact, our DRIFTS studies and catalysis measurements demonstrate the C—H bond scission as the rate determining step in the reaction. The presence of Ni in Cu facilitates the cleavage of C—H bond, thus improving the

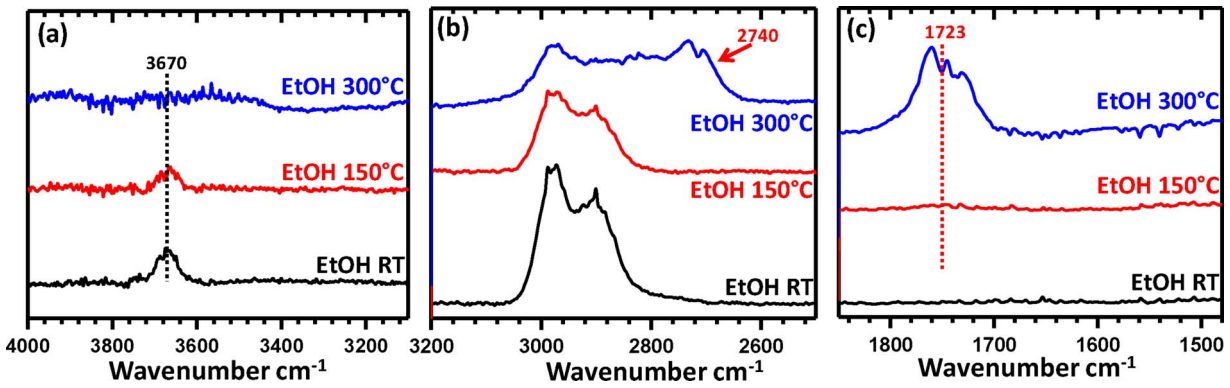

Fig. 9. DRIFT spectra of unsupported np-Cu after exposure to ethanol at various temperatures. (a): spectra in the O—H stretching regime; (b): spectra in the C—H stretching regime; (C) spectra in the C—O stretching regime. See text for details.

catalytic activity of Cu.

DRIFTS tests were also performed on silica supported $Pt_{0.01}Cu$ NPs and $Pd_{0.01}Cu$ NPs after exposure to ethanol at various temperatures. The DRIFTS data on $Pt_{0.01}Cu$ NPs and $Pd_{0.01}Cu$ NPs (not shown here) are similar to supported Cu NPs. The accumulation of adsorbed ethoxy species was also observed on $Pt_{0.01}Cu$ and $Pd_{0.01}Cu$ NPs, suggesting that the presence of isolated Pt or Pd atoms does not significantly improve the activity of Cu in the C−H bond cleavage. Considering that C−H bond cleavage is the rate determining step in ethanol dehydrogenation, such observation is consistent with our catalysis measurements that adding a small amount of Pt or Pd in Cu does not significantly lower the apparent activation energies of Cu in ethanol dehydrogenation. Recently, Marcinkowski et al. have reported that Pt_1Cu SAAs improve the activity of Cu in the dehydrogenation of formic acid to formate by facilitating O−H bond cleavage [28]. However, the presence of Pt in Cu does not improve the activity in the dehydrogenation of formate to CO_2 and H_2, in other words they do not offer a significantly lower barrier for C−H bond cleavage of formate. Such conclusion is in line with our current observation that the presence of Pt does not lower the barrier of C−H bond cleavage of ethanol and therefore does not improve the activity of Cu in ethanol dehydrogenation.

As mentioned above, prior to reduction, the Ni/Cu near surface ratio for $Ni_{0.01}Cu$ materials determined by XPS is 0.12, and after reduction it is 0.06. Likely, before reduction all Ni atoms are present on the surface. Thus, roughly about half of the Ni atoms remain on the surface after reduction and during ethanol dehydrogenation. Assuming the ratio between single Ni atoms and nanoclusters is the same at the surface and subsurface regime, based on XANES data about 35% of Ni species are in single atom form for $Ni_{0.01}Cu$. In this case, about 17.5% of Ni atoms are present on the surface as isolated single atoms for $Ni_{0.01}Cu$, *i.e.* $Ni_{0.00175}Cu$, which has 75% more single surface Ni atoms than the $Ni_{0.001}Cu$ sample, assuming only isolated Ni atoms in $Ni_{0.001}Cu$, all present on the surface. Interestingly, based on the catalysis data we reported before [29], $Ni_{0.01}Cu$ NPs are approximately 55% more active than $Ni_{0.001}Cu$ NPs, at the same reaction conditions, when the rates are normalized per mass of (total) catalyst. Moreover, the same apparent activation energy for ethanol dehydrogenation on $Ni_{0.01}Cu$ NPs and $Ni_{0.001}Cu$ NPs ($\sim$48 kJ/mol) was found, indicating that the active sites and reaction mechanism are similar on these two catalysts. Therefore, combining the characterization data with the catalysis data suggests that for the higher loading $Ni_{0.01}Cu$ catalyst, isolated Ni atoms are the active sites catalyzing the C−H bond cleavage of ethanol, thus significantly increasing the activity of Cu. Consequently, the fraction of Ni species present on the surface as nanoclusters do not change the activity and selectivity of the catalyst, in other words, do not participate in the C−H bond cleavage of ethanol, remaining spectator species during ethanol dehydrogenation, at least in our reaction temperature range ($\leq$300 °C).

It is interesting that adding a small amount of Ni in the Cu surfaces as single isolated Ni atoms can significantly lower the barrier for the activation of C−H bonds. It has been widely reported that metallic Ni is very active for both the C−H bond and C−C bond scission [49,50]. However, in many catalytic reactions, only C−H bond activation is desired, without any C−C bond activation. Thus, in the search for new catalytic materials, it is crucial to find catalyst compositions that are suitable for C−H bond activation, but not active for C−C bond cleavage. Our study has demonstrated that NiCu SAAs meet these criteria, in which Ni atoms in the Cu surface can selectively activate C−H bonds, but different from monometallic Ni NPs, the Ni atoms are inactive for C−C bond cleavage. This unique catalytic activity and selectivity of NiCu SAAs may be extended to other catalytic reactions where C−H bond cleavage is the rate determining step, while C−C bond scission is undesired.

4. Conclusions

We have investigated ethanol dehydrogenation on NiCu SAA alloys, as well as Pt_1Cu and Pd_1Cu SAAs using both kinetic measurements and *in-situ* DRIFTS. Based on EXAFS and XANES studies, Ni is present exclusively as single atoms in $Ni_{0.001}Cu$, while for $Ni_{0.01}Cu$, both Ni single atoms and isolated small nanoclusters are present. Our catalysis measurements show that PtCu and PdCu SAAs do not improve the activity of Cu in ethanol dehydrogenation, whereas adding a small amount of Ni in Cu significantly increases the reactivity of Cu. Through *in-situ* DRIFTS studies, we found that the silica support facilitates the O−H bond scission of ethanol to form the ethoxy intermediate over the supported catalysts, whereas on unsupported nanoporous materials, ethoxy is not detected. Combining DRIFTS studies and catalysis measurements, it can be concluded that the C−H bond scission is the rate determining step in ethanol dehydrogenation. Identification of the rate determining step enables comparison and rank ordering of bimetallic catalysts with optimal properties for alcohol dehydrogenation reactions.

In conclusion, our studies demonstrate that the presence of single atoms of Ni in the Cu surfaces significantly lowers the barrier for C−H bond activation, therefore improving the catalytic activity of Cu in ethanol dehydrogenation. Nickel present as nanoclusters at higher metal loadings is a spectator in the reaction, hence it does not decrease the selectivity to acetaldehyde up to 300 °C. The approach followed in this work can be extended to the investigation of other such systems or reactions involving C−H bond activation, hence it may be of general utility in catalysis. Ni is unique in this reaction as a promoter of Cu, since we found that the PtCu and PdCu SAAs are inferior to NiCu, that is they are similar to monometallic Cu. Such results can guide new computational catalysis studies, aimed at rank ordering these and other bimetallic catalysts.

Acknowledgements

This work was supported as part of the Integrated Mesoscale Architectures for Sustainable Catalysis, an Energy Frontier Research Center funded by the U.S. Department of Energy, Office of Science, Basic Energy Sciences under award #DESC0012573. The XAS research used resources of the Advanced Photon Source, a U.S. Department of Energy (DOE) Office of Science, User Facility operated for the DOE Office of Science by Argonne National Laboratory under Contract No. DE-AC02-06CH11357.

References

[1] M. Eckert, G. Fleischmann, R. Jira, H.M. Bolt, K. Golka, Ullmann's Encyclopedia of Industrial Chemistry, Wiley-VCH Verlag GmbH & Co. KGaA, Weinheim, Germany, 2007.
[2] H.J. Hagemeyer, Acetaldehyde, Kirk Othmer Encyclopedia of Chemical Technology, John Wiley & Sons, Inc., Hoboken, NJ, USA, 2002.
[3] Y.J. Guan, E.J.M. Hensen, Appl. Catal. A-Gen. 361 (2009) 49–56.
[4] F.W. Chang, H.C. Yang, L.S. Roselin, W.Y. Kuo, Appl. Catal. A-Gen. 304 (2006) 30–39.
[5] I.C. Freitas, S. Damyanova, D.C. Oliveira, C.M.P. Marques, J.M.C. Bueno, J. Mol. Catal. A-Chem. 381 (2014) 26–37.
[6] E. Santacesaria, G. Carotenuto, R. Tesser, M. Di Serio, Chem. Eng. J. 179 (2012) 209–220.
[7] Y.J. Tu, Y.W. Chen, Ind. Eng. Chem. Res. 40 (2001) 5889–5893.
[8] F.W. Chang, W.Y. Kuo, K.C. Lee, Appl. Catal. A-Gen. 246 (2003) 253–264.
[9] C.Y. Wang, G. Garbarino, L.F. Allard, F. Wilson, G. Busca, M. Flytzani-Stephanopoulos, ACS Catal. 6 (2016) 210–218.
[10] C.Y. Wang, M. Yang, M. Flytzani-Stephanopoulos, AIChE J. 62 (2016) 429–439.
[11] A. Ciftci, D.A.J.M. Ligthart, P. Pastorino, E.J.M. Hensen, Appl. Catal. B-Environ. 130 (2013) 325–335.
[12] A. Gazsi, A. Koos, T. Bansagi, F. Solymosi, Catal. Today 160 (2011) 70–78.
[13] V.L. Sushkevich, I.I. Ivanova, E. Taarning, ChemCatChem 5 (2013) 2367–2373.
[14] K. Shimizu, K. Sugino, K. Sawabe, A. Satsuma, Chem-Eur. J. 15 (2009) 2341–2351.
[15] R.M. Rioux, M.A. Vannice, J. Catal. 233 (2005) 147–165.
[16] V.Z. Fridman, A.A. Davydov, K. Titievsky, J. Catal. 222 (2004) 545–557.
[17] Y. Ando, M. Yamashita, Y. Saito, Bull. Chem. Soc. Jpn. 76 (2003) 2045–2049.
[18] Q. Fu, H. Saltsburg, M. Flytzani-Stephanopoulos, Science 301 (2003) 935–938.
[19] M. Flytzani-Stephanopoulos, B.C. Gates, Annu. Rev. Chem. Biomol. Eng. 3 (2012)

545–574.
[20] M. Flytzani-Stephanopoulos, Acc. Chem. Res. 47 (2014) 783–792.
[21] J.Y. Liu, ACS Catal. 7 (2017) 34–59.
[22] G. Kyriakou, M.B. Boucher, A.D. Jewell, E.A. Lewis, T.J. Lawton, A.E. Baber, H.L. Tierney, M. Flytzani-Stephanopoulos, E.C.H. Sykes, Science 335 (2012) 1209–1212.
[23] M.B. Boucher, M.D. Marcinkowski, M.L. Liriano, C.J. Murphy, E.A. Lewis, A.D. Jewell, M.F.G. Mattera, G. Kyriakou, M. Flytzani-Stephanopoulos, E.C.H. Sykes, ACS Nano 7 (2013) 6181–6187.
[24] M.B. Boucher, B. Zugic, G. Cladaras, J. Kammert, M.D. Marcinkowski, T.J. Lawton, E.C.H. Sykes, M. Flytzani-Stephanopoulos, Phys. Chem. Chem. Phys. 15 (2013) 12187–12196.
[25] F.R. Lucci, J.L. Liu, M.D. Marcinkowski, M. Yang, L.F. Allard, M. Flytzani-Stephanopoulos, E.C.H. Sykes, Nat. Commun. 6 (2015).
[26] J.L. Liu, F.R. Lucci, M. Yang, S. Lee, M.D. Marcinkowski, A.J. Therrien, C.T. Williams, E.C.H. Sykes, M. Flytzani-Stephanopoulos, J. Am. Chem. Soc. 138 (2016) 6396–6399.
[27] J. Shan, F.R. Lucci, J. Liu, M. El-Soda, M.D. Marcinkowski, L.F. Allard, E.C.H. Sykes, M. Flytzani-Stephanopoulos, Surf. Sci. 650 (2016) 121–129.
[28] M.D. Marcinkowski, J.L. Liu, C.J. Murphy, M.L. Liriano, N.A. Wasio, F.R. Lucci, M. Flytzani-Stephanopoulos, E.C.H. Sykes, ACS Catal. 7 (2017) 413–420.
[29] J. Shan, N. Janvelyan, H. Li, J. Liu, T.M. Egle, J. Ye, M.M. Biener, J. Biener, C.M. Friend, M. Flytzani-Stephanopoulos, Appl. Catal. B: Environ. 205 (2017) 541–550.
[30] M.D. Marcinkowski, A.D. Jewell, M. Stamatakis, M.B. Boucher, E.A. Lewis, C.J. Murphy, G. Kyriakou, E.C.H. Sykes, Nat. Mater. 12 (2013) 523–528.
[31] A. Serov, K. Artyushkova, E. Niangar, C.M. Wang, N. Dale, F. Jaouen, M.T. Sougrati, Q.Y. Jia, S. Mukerjee, P. Atanassov, Nano Energy 16 (2015) 293–300.
[32] N.A. Dhas, C.P. Raj, A. Gedanken, Chem. Mater. 10 (1998) 1446–1452.
[33] Q. Zhu, L.F. Zou, G.W. Zhou, W.A. Saidi, J.C. Yang, Surf. Sci. 652 (2016) 98–113.
[34] N. Becknell, Y.J. Kang, C. Chen, J. Resasco, N. Kornienko, J.H. Guo, N.M. Markovic, G.A. Somorjai, V.R. Stamenkovic, P.D. Yang, J. Am. Chem. Soc. 137 (2015) 15817–15824.
[35] B.C. Gates, H. Knoezinger, F.C. Jentoft, Advances in Catalysis, Elsevier, 2009.
[36] A.N. Mansour, C.A. Melendres, M. Pankuch, R.A. Brizzolara, J. Electrochem. Soc. 141 (1994) L69–L71.
[37] K. Tirez, G. Silversmit, L. Vincze, K. Servaes, C. Vanhoof, M. Mertens, N. Bleux, P. Berghmans, J. Anal. At. Spectrom. 26 (2011) 517–527.
[38] R.T. Mu, Q.A. Fu, H. Xu, H.I. Zhang, Y.Y. Huang, Z. Jiang, S.O. Zhang, D.L. Tan, X.H. Bao, J. Am. Chem. Soc. 133 (2011) 1978–1986.
[39] H.H. Hsieh, Y.K. Chang, W.F. Pong, J.Y. Pieh, P.K. Tseng, T.K. Sham, I. Coulthard, S.J. Naftel, J.F. Lee, S.C. Chung, K.L. Tsang, Phys. Rev. B 57 (1998) 15204–15210.
[40] L.C. Chen, S.D. Lin, Appl. Catal. B-Environ. 148 (2014) 509–519.
[41] L. Pietronero, S. Strassler, Phys. Rev. Lett. 47 (1981) 593–596.
[42] J.S. Lee, Y.S. Lee, T.W. Noh, S. Nakatsuji, H. Fukazawa, R.S. Perry, Y. Maeno, Y. Yoshida, S.I. Ikeda, J.J. Yu, C.B. Eom, Phys. Rev. B 70 (2004).
[43] M.A. Natal-Santiago, J.A. Dumesic, J. Catal. 175 (1998) 252–268.
[44] O. Isaienko, E. Borguet, Opt. Express 20 (2012) 547–561.
[45] J. Rasko, A. Hancz, A. Erdohelyi, Appl. Catal. A-Gen. 269 (2004) 13–25.
[46] R. Asmundsson, P. Uvdal, A.D. MacKerell, J. Chem. Phys. 113 (2000) 1258–1267.
[47] A. Kumar, A. Ashok, R.R. Bhosale, M.A.H. Saleh, F.A. Almomani, M. Al-Marri, M.M. Khader, F. Tarlochan, Catal. Lett. 146 (2016) 778–787.
[48] J.E. Sutton, P. Panagiotopouou, X.E. Veryldos, D.G. Vlachos, J. Phys. Chem. C 117 (2013) 4691–4706.
[49] S.Z. Tasker, E.A. Standley, T.F. Jamison, Nature 509 (2014) 299–309.
[50] X.H. Cai, B. Xie, Arkivoc (2015) 184–211.